Enhanced Red Emission in $CaMoO_4:Bi^{3+},Eu^{3+}$

Suxia Yan,[†,§] Jiahua Zhang,*[,†] Xia Zhang,[†] Shaozhe Lu,[†] Xinguang Ren,[†] Zhaogang Nie,[†,§] and Xiaojun Wang*[,†,‡]

Key Laboratory of Excited State Processes, Changchun Institute of Optics, Fine Mechanics and Physics (CIOMP), Chinese Academy of Sciences, 16 Eastern South Lake Road, Changchun 130033, P. R. China, Graduate School of Chinese Academy of Sciences, Beijing 100039, P. R. China, and Department of Physics, Georgia Southern University, Statesboro, Georgia 30460

Received: May 23, 2007

We report the observation of enhanced red emission at 613 nm originating from $^5D_0 \rightarrow {}^7F_2$ transition of Eu^{3+}-doped $CaMoO_4$ with Bi^{3+} as an additive, under excitation either into the $^5L_6$ state with 395 nm or the $^5D_2$ state with 465 nm. The luminescence properties as a function of Bi^{3+} and Eu^{3+} concentrations are studied. Strongly enhanced red emission of Eu^{3+} is obtained by adding Bi^{3+} instead of increasing the Eu^{3+} concentration. For a fixed Eu^{3+} concentration, there is an optimal Bi^{3+} concentration, at which the maximum luminescence intensity is achieved. The red emission of $CaMoO_4$:0.05Eu^{3+} is enhanced by a factor of 3 as 0.2 Bi^{3+} is co-doped into the system, stronger than that of commercial $Y_2O_2S:Eu^{3+}$ and $Y_2O_3:Eu^{3+}$ phosphors. Lifetime and diffuse reflection spectra measurements indicate that the red emission enhancement is due to the enhanced transition probabilities from the ground state to $^5L_6$ and $^5D_2$ states of Eu^{3+} in the distorted crystal field in which it is considered that more odd-rank crystal field components are induced by crystal structural distortion and symmetry decreasing with the addition of Bi^{3+}, leading to more opposite parity components, for example, $4f^55d$ states, mixed into the $4f^6$ transitional levels of Eu^{3+}. The energy transfer from Bi^{3+} to Eu^{3+} also occurs and is discussed. The present material is a promising red-emitting phosphor for white light diodes with near-UV/blue GaN-based chips.

1. Introduction

Since the realization of GaN-based light emitting diodes (LEDs),[1] more and more interest has been focused on white-light-emitting LED phosphors for the third generation illumination based on UV/blue LEDs, for which many advantages over the present incandescent and fluorescent lamps are expected, such as a long lifetime, high rendering index, high luminosity efficiency, and a concurrent reduction in environment pollution.[2,3]

At present, a white-light LED with a blue InGaN chip (450−470 nm) in combination with a yellow phosphor (YAG:Ce^{3+}) is commercially available.[4] However, such a combination exhibits a poor color rendering index (<80) because of the lack of a red light component (above 600 nm).[5] In addition, the combination of a near-UV InGaN chip (380−410 nm) with blue, green, and red phosphors is another way to generate white light that will yield a high color rendering index and color reproducibility.[6,7] Both applications require red-emitting phosphors, but so far, very limited work involving them has been reported for potential white LED applitions.[8−13] Therefore, it is urgent that efficient red-emitting phosphors suitable for near-UV or blue excitation be researched.

Eu^{3+} (f^6) is a preferable choice as an activator ion with red emission via $^5D_0 \rightarrow {}^7F_2$ transition at about 613 nm, which has been used in most commercial red phosphors.[14] Many scheelite-related phosphors doped with Eu^{3+} have been studied extensively due to their good optical properties.[15−20] In the scheelite-related red phosphors, molybdate (MoO_4^{2-}) is a good choice as a host material. The central Mo^{6+} metal ion is coordinated to four oxygen atoms in tetrahedral symmetry (T_d), and the cations, to eight oxygen atoms from different tetrahedra. Therefore, molybdates are chemically stable, which is better than sulfide and oxysulfide red-emitting phosphors, such as CaS:Eu^{2+} and $Y_2O_2S:Eu^{3+}$. Recently it has been reported that $CaMoO_4:Eu^{3+}$can be effectively excited by near-UV (about 395 nm) and blue (about 465 nm) light, corresponding to the two popular emissions from near-UV and blue LEDs, respectively, and then emits stronger red fluorescence ($^5D_0 \rightarrow {}^7F_2$) than the $CaS:Eu^{2+}$ phosphor used in white-light LEDs.[19] The strong red emission, however, results from the high doping concentration of Eu^{3+} (about 0.24).

In this paper, we report the observation of the red emission enhancement of $CaMoO_4:Eu^{3+}$ by adding Bi^{3+} into the phosphor. Strong red emission can be obtained with Bi^{3+} addition instead of increasing Eu^{3+} concentrations, which is of great value in improving luminescence efficiency of the red phosphor at a much lower cost. The effect of Bi^{3+} on the luminescent properties of $CaMoO_4:Bi^{3+},Eu^{3+}$ is investigated in detail.

2. Experimental

2.1. Sample Preparation. The phosphors $CaMoO_4:Bi^{3+},Eu^{3+}$ have been synthesized by solid-state reaction in air. Stoichiometric mixtures of MoO_3 (A.R), CaO (A.R), Bi_2O_3 (A.R), and Eu_2O_3 (4N) are ground together for 1 h, transferred to an alumina crucible, annealed in a muffle furnace at 700 °C for 8 h by slowly raising the temperature, and cooled slowly to room temperature. The samples are then reground and calcined at

* To whom correspondence should be addressed. Tel: 86-431-86176317. Fax: 86-431-86176317. E-mail: zhangjh@ciomp.ac.cn.
† Key Laboratory of Excited State Physics, Chinese Academy of Sciences.
‡ Georgia Southern University.
§ Graduate School of Chinese Academy of Sciences.

10.1021/jp073991c CCC: $37.00
Published on Web 08/14/2007

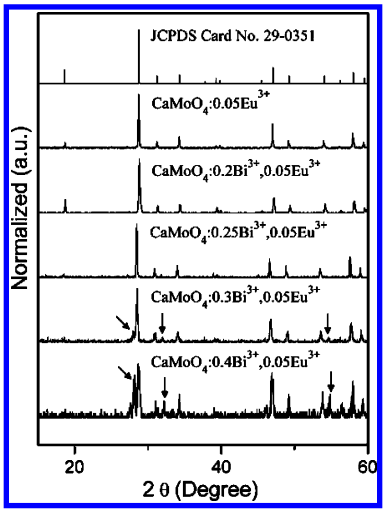

Figure 1. Powder X-ray diffraction patterns of $CaMoO_4:xBi^{3+},0.05Eu^{3+}$ ($x = 0$, 0.2, 0.25, 0.3, and 0.4).

800 °C for 6 h. Finally, the samples are ground into powder for characterizations.

2.2. Characterizations. Phase purities are characterized on a Japan Rigaku D/max-rA powder X-ray diffractometer (XRD) with monochromatized Cu Kα radiation ($\lambda = 0.154\,06$ Å). Photoluminescence (PL) and photoluminescence excitation (PLE) spectra are measured by a Hitachi-4500 fluorescence spectrophotometer equipped with a xenon lamp. The diffuse reflectance measurements are performed using the same spectrometer with $BaSO_4$ powder as a reflectance standard. The lifetimes of the $^5D_0$ state of Eu^{3+} are recorded using the third (355 nm) harmonic of a YAG:Nd pulse laser (Spectra-physics, GCR 130) as the excitation source, and the decay signals are detected with a Tektronix digital oscilloscope mode (TDS 3052). All the measurements are taken at room temperature unless otherwise mentioned.

3. Results and Discussion

3.1. X-ray Diffraction Analysis. The powder X-ray diffraction patterns of $CaMoO_4:xBi^{3+},0.05Eu^{3+}$ with $x = 0$, 0.2, 0.25, 0.3, and 0.4 are shown in Figure 1. It is exhibited that $CaMoO_4:0.05Eu^{3+}$ forms a scheelite phase that has a tetragonal unit cell with space group $I4_1/a$, $Z = 4$ (JCPDS card no. 29-0351).[21] When Bi^{3+} is added into $CaMoO_4:Eu^{3+}$ with the content $x \leq 0.25$, the samples are basically single phase with a tetragnal crystal structure, indicating that the samples form solid solutions. It is also found that the XRD peaks of Bi_2O_3 clearly appear when Bi^{3+} content is higher than 0.25, implying the occurrence of solubility saturation.

As we know, both the ionic radii of Eu^{3+} ($r = 1.07$ Å when coordination number (CN) = 8) and Bi^{3+} ($r = 1.17$ Å when CN = 8) are close to that of Ca^{2+} ($r = 1.12$ Å when CN = 8), and the four coordinated Mo^{6+} ($r = 0.41$ Å when CN = 4) sites are too small for Eu^{3+} or Bi^{3+} to occupy.[22] We therefore believe that Eu^{3+} and Bi^{3+} ions prefer to occupy the Ca^{2+} sites.[23,24] Generally, when a metal ion is substituted for an element with a different valency in the matrix, charge compensation is needed using ions such as Na^+ or Li^+.[25] In our present work, the phosphors are synthesized without any charge compensation ions, and structures obtained are still consistent with the scheelite phase with Bi^{3+} content $x \leq 0.25$. Therefore, we assume that the charge loss is most probably compensated by Ca^{2+} vacancies (V_{Ca}) described by

$$3Ca^{2+} \rightarrow 2Eu^{3+} + V_{Ca}$$

and

$$3Ca^{2+} \rightarrow 2Bi^{3+} + V_{Ca}$$

With Bi^{3+} as an additive, the diffraction peaks have a blue shift. When Bi^{3+} content is more than 0.25, the XRD peaks broaden. It is assumed to be caused by the generation of V_{Ca}, and the different ion radii of Ca^{2+}, Bi^{3+}, and Eu^{3+}, which may modify the crystal structure or distort the metal oxide polyhedrons.[23]

3.2. PL and PLE Properties of $CaMoO_4:xBi^{3+},0.05Eu^{3+}$ as a Function of Bi^{3+} Concentrations. The PL spectra of $CaMoO_4:0.2Bi^{3+},0.05Eu^{3+}$ and $CaMoO_4:0.05Eu^{3+}$ are presented in Figure 2. The PL spectra show a strong emission line at 613 nm and a weak emission at 593 nm, which arise from the $^5D_0 \rightarrow {}^7F_2$ and the $^5D_0 \rightarrow {}^7F_1$ transitions of Eu^{3+}, respectively.[26] It is observed that the addition of Bi^{3+} has no effect on the shape of the PL spectra of $CaMoO_4:0.05Eu^{3+}$, but greatly enhances the PL intensity.

Curves a−f presented in Figure 3 are PLE spectra of Eu^{3+} in $CaMoO_4:xBi^{3+},0.05Eu^{3+}$ monitoring the $^5D_0 \rightarrow {}^7F_2$ emission with different Bi^{3+} concentrations ($x = 0$, 0.05, 0.1, 0.2, 0.25, and 0.3). The PLE spectra show characteristic intra-4f transition lines of Eu^{3+}: $^7F_0 \rightarrow {}^5D_2$ (465 nm) and $^7F_0 \rightarrow {}^5L_6$ (395 nm) along with a broad $O^{2-}-Eu^{3+}$ charge-transfer (CT) band in the UV region. The PLE spectrum of singly doped $CaMoO_4:Eu^{3+}$ (curve a) depicts weak $^7F_0 \rightarrow {}^5D_2$ and $^7F_0 \rightarrow {}^5L_6$ excitation lines as well as a strong CT band centered at ~280 nm. As is Bi^{3+} incorporated, especially for the concentration $x = 0.2$, the $^7F_0 \rightarrow {}^5L_6$ and $^7F_0 \rightarrow {}^5D_2$ transitions are greatly enhanced (curve d). A new PLE band also appears at ~330 nm, as represented in curves b−f. The new PLE band is experimentally evidenced as the absorption of Bi^{3+} based on the PLE spectrum of Bi^{3+} singly doped $CaMoO_4$ (curve g). Bi^{3+} ion is a mercury-like ion with a $6s^2$ configuration, and its luminescence properties depend strongly on the composition and crystal structure of the host. The electronic configuration of Bi^{3+} is composed of the ground state $6s^2$ and the first excited state 6s6p,[27] which emits blue fluorescence at 480 nm in $CaMoO_4$, as shown as an insert of spectrum g in Figure 3. The excitation spectrum for the 480 nm emission of Bi^{3+} exhibits a band centered around 330 nm, which is consistent with the new PLE band in Bi^{3+}- and Eu^{3+}-co-doped $CaMoO_4$, suggesting the occurrence of energy transfer from Bi^{3+} to Eu^{3+}.[28,29]

Figure 4 depicts the dependence of the Eu^{3+} emission intensities on Bi^{3+} concentration in $CaMoO_4:xBi^{3+},0.05Eu^{3+}$ ($x = 0$, 0.01, 0.05, 0.1, 0.15, 0.2, 0.25, 0.3, and 0.4) under 395 and 465 nm excitations, respectively. The emission intensities initially increase with increasing Bi^{3+} concentration and reach a maximum around $x = 0.2$.

3.3. Mechanism of Luminescence Enhancement of Eu^{3+}. To understand whether the increase of the $^5D_0 \rightarrow {}^7F_2$ emission intensity of Eu^{3+} is due to the increase of the quantum efficiency of $^5D_0 \rightarrow {}^7F_2$ emission of Eu^{3+} or the absorption strength of $^7F_0 \rightarrow {}^5L_6$ and $^7F_0 \rightarrow {}^5D_2$ transitions, the lifetimes of the $^5D_0$ state of Eu^{3+} and the diffuse reflection spectra of $CaMoO_4:xBi^{3+},0.05Eu^{3+}$ ($x = 0-0.4$) are measured, as shown in Figure 5and Figure 6, respectively. In Figure 5, the lifetime of $^5D_0$ reduces slightly with increasing Bi^{3+} concentration, indicating that the quantum efficiency of $^5D_0 \rightarrow {}^7F_2$ emission is hardly affected by Bi^{3+} addition. Therefore, it hints that the Bi^{3+}-induced red emission enhancement may result from the increase of the $^7F_0 \rightarrow {}^5L_6$ and $^7F_0 \rightarrow {}^5D_2$ absorption strengths.

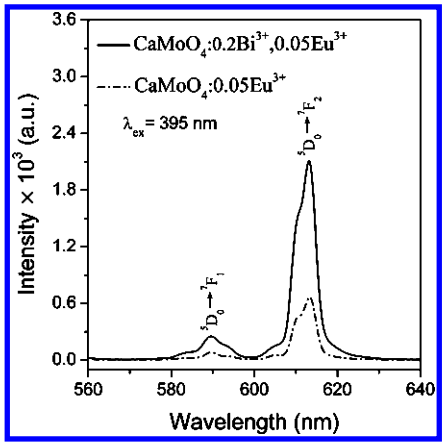

Figure 2. Comparison of PL spectra of $CaMoO_4$:0.05Eu^{3+} and $CaMoO_4$:0.2Bi^{3+},0.05Eu^{3+} under 395 nm excitation.

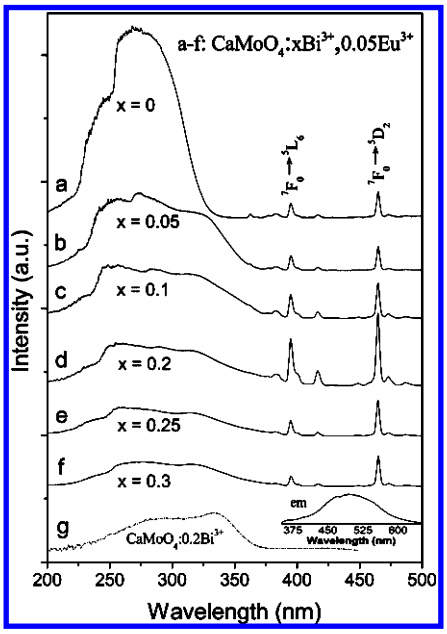

Figure 3. PLE spectra of $CaMoO_4$:xBi^{3+},0.05Eu^{3+} (x = 0, 0.05, 0.1, 0.2, 0.25, and 0.3, for curves a−f, respectively), monitoring the 613 nm Eu^{3+} emission ($^5D_0 \rightarrow {}^7F_2$). (g) PLE spectrum of $CaMoO_4$:0.2Bi^{3+} for monitoring the emission of Bi^{3+} at 480 nm; inset: emission (em) spectra of Bi^{3+} in $CaMoO_4$ under 330 nm excitation.

In Figure 6, the absorption peaks of intra-4f transitions of Eu^{3+} at 395 and 465 nm are presented. The absorbance increases with increasing Bi^{3+} content and reaches the maximum when the concentration of Bi^{3+} $x = 0.2$, which evidences that the enhancement of the $^5D_0 \rightarrow {}^7F_2$ emission of Eu^{3+} is caused mainly by the increase of absorption strength of $^7F_0 \rightarrow {}^5L_6$ and $^7F_0 \rightarrow {}^5D_2$ transitions. It is also observed in Figure 6 that, in addition to the $O^{2-}-Eu^{3+}$ CT absorption band at 280 nm, the absorption band at around 330 nm arising from Bi^{3+} also appears as Bi^{3+} is added. In addition, with increasing concentrations of Bi^{3+}, the absorption band of Bi^{3+} shows a red shift that has not been observed in the PLE spectra (Figure 3). The shift can be attributed to the aggregation of Bi^{3+} centers at higher concentrations, lowering the absorption energy compared to single Bi^{3+} ions.[30] These Bi^{3+} aggregates may quench the absorbed excitation energy rather than transfer to Eu^{3+}, leading to no red shift in the PLE spectra.

In view of the change of the $^7F_0 \rightarrow {}^5L_6$ and $^7F_0 \rightarrow {}^5D_2$ absorption strength of Eu^{3+} as a function of Bi^{3+} concentration (Figure 6), we believe that in the $CaMoO_4$:Eu^{3+} lattice, the incorporation of Bi^{3+} ions destroys the crystal symmetry of

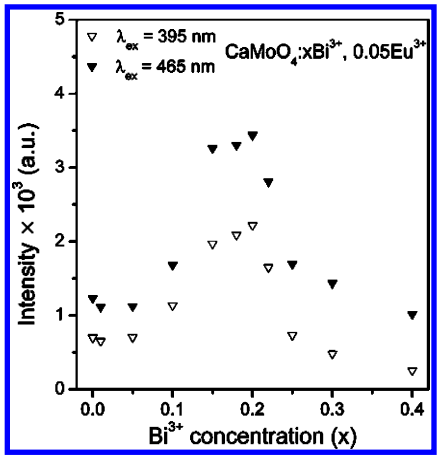

Figure 4. Bi^{3+} concentration (x) dependence of the PL intensities of Eu^{3+} ($^5D_0 \rightarrow {}^7F_2$) in $CaMoO_4$:xBi^{3+},0.05Eu^{3+} under excitation at 395 and 465 nm, respectively.

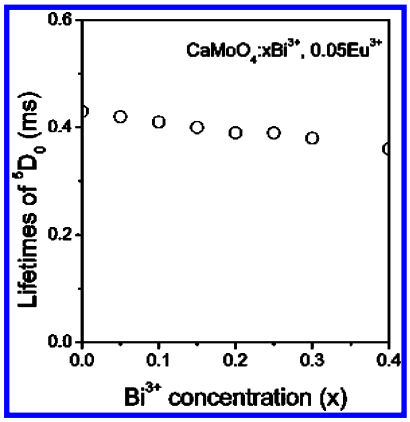

Figure 5. Dependence of lifetimes of the $^5D_0$ state of Eu^{3+} in $CaMoO_4$:xBi^{3+},0.05Eu^{3+} on Bi^{3+} concentration (x).

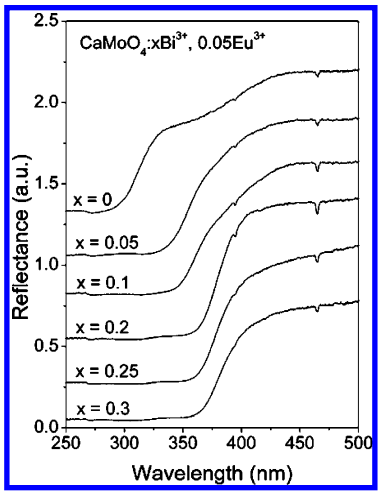

Figure 6. Diffuse reflection spectra of $CaMoO_4$:xBi^{3+},0.05Eu^{3+} at various concentrations of Bi^{3+} (x).

Eu^{3+}. On one hand, the distortion is due to the bigger radius of Bi^{3+} (r = 1.17 Å when CN = 8) compared to Eu^{3+} (r = 1.07 Å when CN = 8) and Ca^{2+} (r = 1.12 Å when CN = 8). On the other hand, the charge compensation for Bi^{3+} substituting for a Ca^{2+} site leads to the generation of Ca^{2+} vacancies and other point defects, which also distorts the crystal field around Eu^{3+}.[31] On the analysis above, it is therefore speculated that more odd-rank crystal field components are induced by crystal structural distortion and symmetry decreasing with the addition of Bi^{3+}, leading to more opposite parity components, namely, $4f^55d$

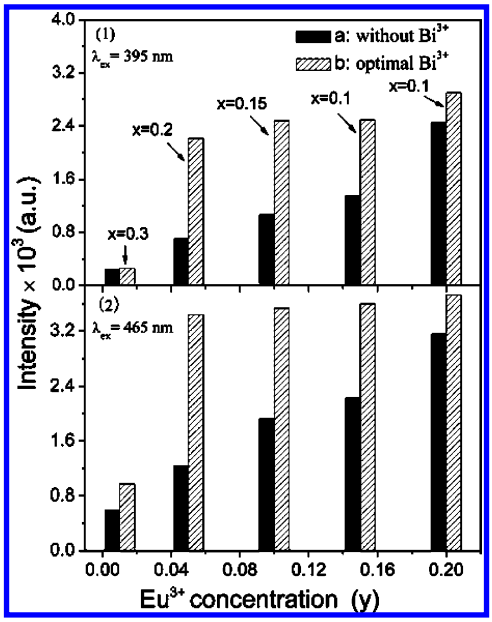

Figure 7. Comparison of the PL intensities in Eu^{3+} singly doped and Eu^{3+} and Bi^{3+} co-doped $CaMoO_4$ with optimal Bi^{3+} concentration at each fixed Eu^{3+} concentration under (1) 395 nm and (2) 465 nm excitation.

states, mixed into the $4f^6$ transitional levels of Eu^{3+}. This may result in the enhancement of the intra $4f^6$ transition probability of Eu^{3+} ($^7F_0 \rightarrow {}^5L_6$ and $^7F_0 \rightarrow {}^5D_2$).

For the optimal Bi^{3+} content $x = 0.2$ in $CaMoO_4$:$x$$Bi^{3+}$,0.05$Eu^{3+}$ material, we know from the XRD patterns in Figure 1 that Bi_2O_3 can no longer be soluble in $CaMoO_4$:0.05Eu^{3+} when the content of Bi^{3+} is more than 0.25. As the result, the Bi^{3+} content of 0.2 is around the solubility limit, beyond which the extra Bi_2O_3 cannot incorporate into the host lattices, resulting in a decrease in luminescence.

3.4. Comparison of Luminescence Intensities of $CaMoO_4$:$x$$Bi^{3+}$,$y$$Eu^{3+}$ with $CaMoO_4$:$y$$Eu^{3+}$ at Various Eu^{3+} and Bi^{3+} Concentrations. The luminescence intensities of Eu^{3+} singly doped $CaMoO_4$ and Eu^{3+}, Bi^{3+} co-doped $CaMoO_4$ as a function of Eu^{3+} and Bi^{3+} concentrations are studied. It is found in Eu^{3+} and Bi^{3+} co-doped $CaMoO_4$ that for each fixed Eu^{3+} concentration, there is a corresponding optimal Bi^{3+} concentration for the red emission enhancement. Figure 7 illustrates the optimal Bi^{3+} concentrations that maximize the red emission enhancement for different Eu^{3+} concentrations ($y = 0.01$, 0.05, 0.1, 0.15, and 0.2) under 395 nm excitation (1) and 465 nm excitation (2). It is clear that adding Bi^{3+} enhances the red emission intensities for every Eu^{3+} concentration investigated, with better efficiency at lower Eu^{3+} concentration. The most efficient concentrations occur at $y = 0.05$ and $x = 0.2$, which intensifies the PL emission by a factor of 3, close to the intensity of $y = 0.2$ without Bi^{3+} addition ($x = 0$). The graphs also show that the optimal Bi^{3+} concentration is dependent on the Eu^{3+} concentration. The lower (higher) the Eu^{3+} concentration is doped, the higher (lower) the optimal Bi^{3+} concentration that is required. It is also observed in Figure 7 that the total combined concentration of Bi^{3+} and Eu^{3+} remains in the range of ~0.25−0.3, which means the maximum soluble content of these trivalent ions in the $CaMoO_4$ host. In other words, the optimal concentration is total-solubility-manipulated. It is therefore understandable that strong red emission can be obtained by adding Bi^{3+} instead of increasing the Eu^{3+} concentration, which is of great value in improving luminescence efficiency of the red phosphor at a much lower cost.

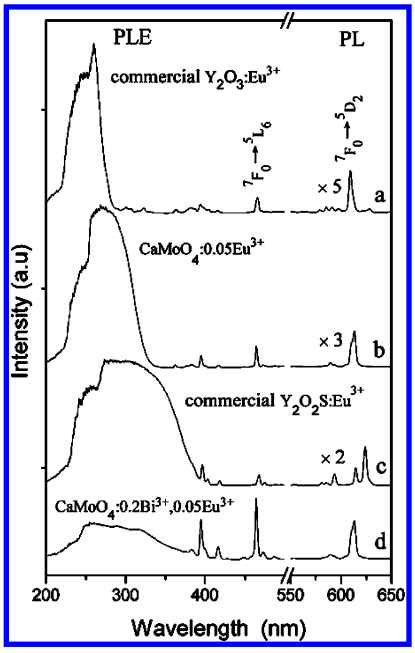

Figure 8. PLE monitoring the red emission of Eu^{3+} in (a) commercial Y_2O_3:Eu^{3+} ($\lambda_{em} = 610$ nm), (b) $CaMoO_4$:0.05Eu^{3+} ($\lambda_{em} = 613$ nm), (c) commercial Y_2O_2S:Eu^{3+} ($\lambda_{em} = 624$ nm), and (d) $CaMoO_4$:0.2Bi^{3+},0.05Eu^{3+} ($\lambda_{em} = 613$ nm), and PL spectra under 395 nm excitation.

3.5. Comparison of Luminescence Intensities of $CaMoO_4$:$x$$Bi^{3+}$,$y$$Eu^{3+}$ with Commercial Red Phosphors. With the purpose of red phosphor application for white-light LEDs with near-UV/blue GaN-based chips as excitation sources, the PL spectra upon 395 nm excitation into the $^5L_6$ state and the PLE spectra monitoring the red emission in $CaMoO_4$:$x$$Bi^{3+}$,0.05$Eu^{3+}$ are compared with that of commercial Y_2O_3:Eu^{3+} (sample a) and Y_2O_2S:Eu^{3+} (sample c) red phosphors, as shown in Figure 8. Of these materials, $CaMoO_4$:0.2Bi^{3+},0.05Eu^{3+} (sample d) exhibits the strongest red emission. Under 395 excitation, the red emission of $CaMoO_4$:0.2Bi^{3+},0.05Eu^{3+} is about 2 and 5 times stronger than that of Y_2O_2S:Eu^{3+} and Y_2O_3:Eu^{3+}, respectively. It is also demonstrated in the PLE spectra that the $^7F_0 \rightarrow {}^5D_2$ intensity in $CaMoO_4$:0.2Bi^{3+},0.05Eu^{3+} is about 5 and 4 times stronger than the corresponding peaks of Y_2O_2S:Eu^{3+} and Y_2O_3:Eu^{3+}, respectively, indicating that $CaMoO_4$:Bi^{3+},Eu^{3+} is a promising red phosphor for white-light LEDs.

4. Conclusions

In conclusion, addition of Bi^{3+} strongly enhances the red emission of Eu^{3+} ($^5D_0 \rightarrow {}^7F_2$) in $CaMoO_4:Bi^{3+},Eu^{3+}$ under excitations of 395 and 465 nm that correspond to the two popular lines emitted from UV and blue LED, respectively, making the co-doped $CaMoO_4:Bi^{3+},Eu^{3+}$ a very promising phosphor for white-light LED applications. For each Eu^{3+} concentration, an optimal Bi^{3+} concentration is found to maximize the red emission. The most efficient concentrations for the maximum red emission occur at 0.05 and 0.2 for Eu^{3+} and Bi^{3+}, respectively, with the red emission stronger than commercial Y_2O_2S:Eu^{3+} and Y_2O_3:Eu^{3+} phosphors. The enhanced red emission is attributed to the enhanced f−f absorption of Eu^{3+}. It is speculated that more odd-rank crystal field components are induced by crystal structural distortion and symmetry decreasing with adding Bi^{3+}, leading to more opposite parity components, forexample, $4f^55d$ states, mixed into the $4f^6$ transitional levels of Eu^{3+}. The existence of optimal Bi^{3+} concentration for a fixed Eu^{3+} concentration is due to the

existence of maximum soluble content of these trivalent ions in the $CaMoO_4$ host.

Acknowledgment. This work is financially supported by the MOST of China (2006CB601104, 2006AA03A138) and the National Natural Science Foundation of China (10574128).

References and Notes

(1) Nakamura, S.; Senoh, M.; Mukai, T. *Appl. Phys. Lett*. **1993**, *62*, 2390.
(2) Narendran, N.; Maliyagoda, N.; Bierman, A.; Pysar, R. M.; Overington, M. *Proc. SPIE* **2000**, *3938*, 240.
(3) Brown, M. *Proc. SPIE* **2001**, *4445*, 49.
(4) Nakamura, S.; Fasol, G. *The Blue Laser Diode*; Springer: Berlin, 1997.
(5) Ponce, F. A.; Bour, D. P. *Nature* (London) **1997**, *386*, 351.
(6) Park, J. K.; Lim, M. A.; Kim, C. H.; Park, H. D.; Park, J. T.; Choi, S. Y. *Appl. Phys. Lett.* **2003**, *82*, 683.
(7) Huh, Y. D.; Shim, J. H.; Kim, Y.; Do, Y. R. *J. Electrochem. Soc.* **2003**, *150*, H57.
(8) Nishida, T.; Ban, T.; Kobayashi, N. *Appl. Phys. Lett.* **2003**, *82*, 3817.
(9) Wang, Z. L.; Liang, H. B.; Zhou, L. Y.; Wu, H.; Gong, M. L.; Su, Q. *Chem. Phys. Lett.* **2005**, *412*, 313.
(10) Sohn, K. S.; Park, D. H.; Cho, S. H.; Kwak, J. S.; Kim, J. S. *Chem. Mater.* **2006**, *18*, 1768.
(11) Chi, L. S.; Liu, R. S.; Lee, B. J. *J. Electrochem. Soc.* **2005**, *152*, J93.
(12) Xie, R. J.; Hirosaki, N.; Suehiro, T.; Xu, F. F.; Mitomo, M. *Chem. Mater*. **2006**, *18*, 5578.
(13) Piao, X.; Horikawa, T.; Hanzawa, H.; Machida, K. I. *Appl. Phys. Lett.* **2006**, *88*, 161908.
(14) Ronda, C. R. *J. Lumin.* **1997**, *72*, 49.
(15) Van Uitert, L. G.; Soden, R. R.; Linares, R. C. *J. Chem. Phys.* **1962**, *36*, 1793.
(16) Torardi, C. C.; Page, C.; Brixner, L. H.; Blasse, G.; Dirksen, G. J. *J. Solid State Chem.* **1987**, *69*, 171.
(17) Kim, T.; Kang, S. *J. Lumin*. 2007, *122*−*123*, 964.
(18) Neeraj, S.; Kijima, N.; Cheetham, A. K. *Chem. Phys. Lett.* **2004**, *387*, 2.
(19) Hu, Y. S.; Zhuang, W. D.; Ye, H. Q.; Wang, D. H.; Zhang, S. S.; Huang, X. W. *J. Alloys Compd.* **2005**, *390*, 226.
(20) Wang, Z. L.; Liang. H. B.; Wang, J.; Gong, M. L.; Su, Q. *Appl. Phys. Lett.* **2006**, *89*, 071921.
(21) Gürmen, E.; Deniels, E.; King, J. S. *J. Chem. Phys.* **1971**, *55*, 1093.
(22) Shannon, R. D. *Acta Crystallogr*. 1976, *A32*, 751.
(23) Yao, W. F; Ye. J. H. *J. Phys. Chem. B* **2006**, *110*, 11188.
(24) Fu, Z. L.; Zhou, S. H.; Yu, Y. N.; Zhang, S. Y. *J. Phys. Chem. B* **2005**, *109*, 23320.
(25) Wang, J. G.; Jing, X. P.; Yan, C. H.; Lin, J. H. *J. Electrochem. Soc.* **2005**, *152*, G186.
(26) Jia, W. Y.; Liu, H. M.; Felofilov, S. P.; Meltzer, R.; Jiao, J. *J. Alloys Compd.* **2000**, *311*, 11.
(27) Shin, S. H.; Jeon, D. Y.; Suh, K. S. *J. Appl. Phys.* **2001**, *90*, 5986.
(28) Blasse, G.; Bril, A. *J. Chem. Phys.* **1967**, *47*, 1920.
(29) Neeraj, S.; Kijima, N.; Cheetham, A. K. *Solid State Commun.* **2004**, *131*, 65.
(30) Pode, R. B.; Dhoble, S. J. *Phys. Status Solidi B* **1997**, *203*, 571.
(31) Su. Q.; Pei, Z. W.; Chi, L. S.; Zhang, H. J.; Zhang, Z. Y.; Zou, F. *J. Alloys Compd*. **1993**, *192*, 25.